

## THE INFLUENCE OF CERAMIC PARTICLES ON THE CORROSION PROPERTIES OF NOVEL Ti750 MATRIX ALLOY

Vitus Mwinteribo TABIE<sup>1\*</sup>, James Kwasi QUAISIE<sup>2</sup>, Jianwei LI<sup>3</sup>,  
Philip YAMBA<sup>2</sup>, Xiaojing XU<sup>3</sup>

<sup>1</sup>Department of Mechanical Engineering, Hilla Limann Technical University, Ghana

<sup>2</sup> Faculty of Engineering, Tamale Technical University, Ghana

<sup>3</sup> Institute for Advanced Manufacturing and Modern Equipment Technology,  
Jiangsu University, Zhenjiang, Jiangsu 212013, PR China

### Abstract

*This paper explores the corrosion behavior of matrix Ti750 alloy and its composites prepared using SiCp, B<sub>4</sub>C, SiCw, and GPLs particles as reinforcement. The consolidation of the metallic powders was by spark plasma sintering method. The study chose mixed molten salt of 25% NaCl + 75% Na<sub>2</sub>SO<sub>4</sub> as the corrosive medium and the hot corrosion behavior of the solid-solution aging at 800 °C. The study found that at the same corrosion temperature, the rate of change of the weight gain curves of all the materials was similar. The corrosion weight gain of the base material was the highest (14.10 mg.cm<sup>-2</sup>), while the 5vol.% SiCp reinforced composite had the lowest weight gain of 5.1 mg.cm<sup>-2</sup>, which is 36.17% of the base alloy. The corrosion products of all the materials were mainly composed of TiO<sub>2</sub>, Al<sub>2</sub>O<sub>3</sub>, Na<sub>2</sub>TiO<sub>3</sub>, and Al<sub>2</sub>TiO<sub>5</sub>. The peak of SiO<sub>2</sub> was enhanced when SiCp was added, and there was no distinct peeling off of the corrosion layers, unlike the base material, which had partial shedding, deep cracks, and holes. The 5vol.% SiCp reinforced composite therefore possessed the best corrosion performance.*

**Keywords:** Ti750 Matrix Alloy, Ceramic Particles, Powder Metallurgy, Corrosion, Spark plasma sintering (SPS)

### Introduction

Titanium alloys and composites are promising materials for aircraft engine design because of their excellent properties at elevated temperatures up to 600 °C [1-4]. Beyond this temperature, however, the Ti element combines with oxygen to yield non-protective oxide scales [5,6]. The Ti-Al-Sn-Zr-Mo-Si series alloys, in consolidation with  $\beta$ -stabilizers and appropriate thermomechanical processing, can attain 650 °C - 700 °C operating temperatures [7-9]. The Chinese Academy of Sciences developed a Ti-Al-Sn-Zr-Mo-Si series alloy, also known as Ti750, which can operate at 700°C - 750°C for a brief period [10]. With a good amount of  $\alpha$  phase, the Ti750 has Ti-6Al-4Sn-9Zr-1.21Nb-1.6Mo-0.3Si nominal composition. The contents of Al and Sn produce a large significant amount of ordered  $\alpha$  phases of Ti<sub>3</sub>X (Al and Sn) precipitates at high temperatures [11,12]. Controlling the distribution and amount of these precipitates leads to improve strength and plasticity of the alloy [12]. Jayaprakash et al. [13] found that additions of Zr to this series of Ti alloys enhanced strength at both room and high temperatures. It can form very stable precipitates with Si and Ti at 650 °C. Nb promotes the formation of ternary silicides such as (TiZr)<sub>6</sub>Si<sub>3</sub>, which enhances the fracture toughness of near  $\alpha$  Ti alloys [14]. Chen et al. [15] have demonstrated that Mo contents in Ti750 alloy indirectly increase the thermodynamic stability of the alloy. Si is an indispensable element for many high-temperature Ti alloys because

\*Corresponding author: tabieson@yahoo.com

it forms silicides, which disperse in the alloy and hinder the movement of dislocations. A 0.1%~0.5% addition of Si in high-temperature Ti alloys improves the strength and high-temperature creep resistance [16].

Although titanium, its alloys, and composites have low density, high specific strength, Young's modulus, and other excellent mechanical and corrosion resistance properties, there exist limitations in some aspects. Certain defects, such as low hardness, abrasion resistance, poor mechanical properties, and poor corrosion and oxidation resistance at higher temperatures, have severely impeded the implementation of the material in engineering. The particle reinforcements in the titanium matrix can effectively boost the mechanical properties and high-temperature materials' resistance to corrosion and oxidation, thereby subduing some performance defects of the titanium alloy. For example, Poletti and Höltl [17] used SiC, TiB whiskers, and TiC particles to reinforce Ti alloys and the developed composites had superior strength than the base materials. The oxidation behavior of TMCs reinforced with particles was also studied by Qin et al.[18]. They observed that the TiC particle reinforcement has lower oxidation at 550 °C, 600 °C, and 650 °C. Kim et al. [19] also used TiB and TiC reinforcements for Ti alloy, and the resulting TMCs had higher oxidation resistances. Preliminary studies by Tabie et al. [20] on SiCp, B<sub>4</sub>C, SiCw, and GPLs reinforced Ti750 alloy also yielded lower oxidation weight gains compared to the matrix alloys. Several studies have also evaluated the corrosion performance of particle-reinforced Ti alloys [21-23]. The composites demonstrated excellent resistance to corrosion than the base alloys. Therefore, particle-reinforced titanium-based composites have broad research and application prospects. Currently, many pieces of research are focused on particles-reinforced titanium-based composites synthesized using powder metallurgy.

Spark plasma sintering (SPS) is the most commanding powder metallurgical technique [24-27]. The technology produces high-density components with near-net-shapes within a few minutes through the localized plastic movement of the connected particles [24]. Besides, it is very efficient, requires low processing temperature, energy-saving, less grain growth, and less pollutant [26,27].

When Ti alloys and their composites are used at extreme temperatures above 600 °C and in working environments with impurities such as sulfur, sodium, chlorine, and oxygen, thermal corrosion occurs. Thermal corrosion of materials accelerates under the combined action of oxygen and other corrosive gases leading to corrosion damages [28]. It causes damage to the interior material's composition, and the mechanical characteristics, are significantly reduced, which severely weakens the material's performance. Therefore, studying the thermal corrosion behavior of titanium-based composite materials, exploring the mechanism of thermal corrosion generation, and seeking effective means to suppress the occurrence of thermal corrosion is of great significance to enhance the material's performance.

## Materials and Methods

The experiment used SiCp, B<sub>4</sub>C, SiCw, and GPLs granulates as reinforcements for Ti750 matrix alloy. The TMCs were prepared first by mechanical ball milling the powders, followed by consolidation using the spark plasma sintering method. For comparison purposes, the base alloy, Ti750, was fabricated by the same process. The schematic of the experimental procedure is shown in Fig. 1. Table 1 shows all the materials and chemicals used in this experiment. They were all procured from Jiangsu Vilory Advanced Materials Technology Co., Ltd- PR China. The scanned microstructures of the raw materials powder (Fig. 2) were analyzed using the SPECTRO MAXx spectrometer.

**Table 1.** List of experiment materials.

Chemical/Material	Particle size ( $\mu\text{m}$ )	Purity (wt.%)
Pre-alloyed Ti750	10 –90	>99
SiC particles	50	>99.9
Boron carbide ( $\text{B}_4\text{C}$ )	60	>99.9
SiC whiskers	$L \geq 2, D = 0.1 - 2.5$	>99.9
Graphene particles (GPLs)	$L = 0.5 - 5, D = 0.7 - 1.2$	>98
Sodium sulfate ( $\text{Na}_2\text{SO}_4$ )		>99
Sodium chloride ( $\text{NaCl}$ )		>99
Nitric acid ( $\text{HNO}_3$ )		>99
Hydrofluoric acid ( $\text{HF}$ )		>99

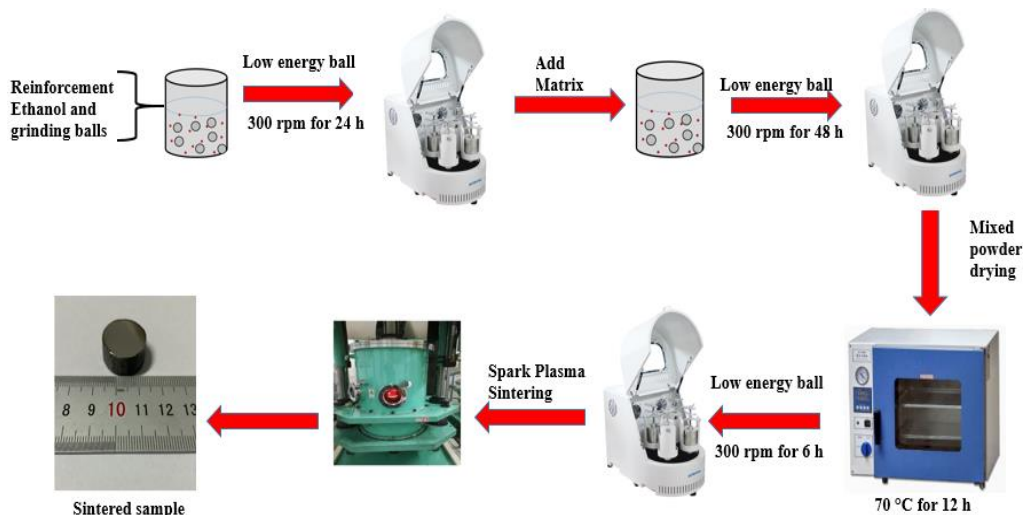


**Fig. 1.** schematic diagram of the experimental process.

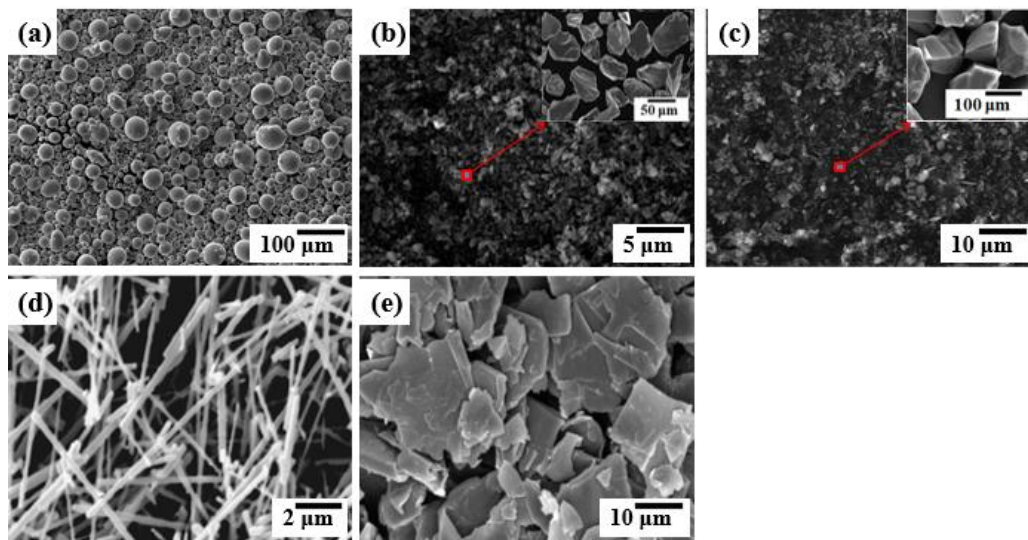


**Fig. 2.** Microstructure of the raw materials: (a) Atomized Ti750 alloy powder, (b)  $\text{B}_4\text{C}_p$  (c)  $\text{SiC}_p$  (d)  $\text{SiC}_w$ , and (e) GNPs[29]

The experiment used a planetary ball mill with model number QM-3SP4 manufactured by Nanjing T-Bota Sciotech Instruments and Equipment Company to mill the raw material powder. The powder-to-ball ratio was 8:1, and that of big balls to small balls was 1:4. A low-energy ball milling at 300 r/min was used to mix the raw powders for 24 h. The mixing was thorough to achieve uniform distribution of reinforcements in the matrix and avoid a reduction in the compressibility of mixed powders [30]. The reinforcements were first measured into the mill tank and submerged in pure ethanol to about 2/3 of the mill tank volume. The powder formulation in Table 2 was developed using the optimum performance ratios of the reinforcement materials from literature and testing and comparing the mechanical properties of a series of samples with different volume fractions. An Ohaus discovery optical balance with a precision of ±2 mg was used to weigh the powders.

Table 2. TMC powders chemical composition.

Sample	Constituents (vol. %)				Matrix alloy
	SiC <sub>w</sub>	B <sub>4</sub> C	GPLs	SiC <sub>p</sub>	
A	0	0	0	0	bal
B	0	1	0	5	bal
C	5	0	0	5	bal
D	0	0	0.15	5	bal
E	0	0	0	5	bal

The ball milled powder was subjected to spark plasma sintering (SPS) using the DR.SINTER-type SPS-3.20 discharge plasma sintering furnace with the heating rate was set to 100 °C/min, the pressure 50 MPa, the holding time 10min, the sintering temperature 1350 °C, and the furnace cooled after the heating. The sintered samples have diameters of 20 mm and a height of 30 mm

The sintered samples were cut into 7mm × 7mm × 5mm small test samples. All six surfaces of the sample were polished and ultrasonically cleaned. The experiment selected a box-type resistance furnace, SX2-4-10 model, used the salt coating method, weighed the samples with an optical balance (accuracy 0.0001g), and the corrosive solution was 25% NaCl and 75% Na<sub>2</sub>SO<sub>4</sub> aqueous solution. The temperature was set at 800 °C, and the corrosion time to 30h. At 0h, 1h, 3h, 5h, 7h, 10h, 15h, 20h, 25h, and 30h, corrosion times, the sample was taken out of the crucible and weighed. The corrosion gain of the sample was measured to obtain the corrosion kinetic curve. The corrosion products' XRD pattern after thermal corrosion was analyzed. The samples' surface morphology and cross-section were observed using electron microscopy.

## Results and discussion

### Corrosion kinetics analysis after 30 hours of hot corrosion

The corrosion gain curves of the matrix and composite materials after thermal corrosion at 800 °C for 30 hours are shown in Fig. 3. It can be seen from the Fig. that at the same corrosion temperature, the thermal corrosion kinetics curves of all the materials are similar. Initially, the corrosion weight of the material increased significantly, and the reaction on the surface was intense. The slope of the curve reduced significantly after 5 hours of hot corrosion, and the corrosion rate became lower than in the initial stage. As time increases, the material's corrosion weighting curve gradually flattens, and the corrosion reaction progresses very slowly.

Comparing the corrosion kinetics curves of the materials at the same temperature found that the corrosion gain of the base alloy was the highest. The corrosion gain of the base alloy after corrosion at 800 °C for 30 hours was 14.10 mg.cm<sup>-2</sup>. The 5vol.% SiC<sub>p</sub> reinforced composite had the lowest weight gain after corrosion at 800 °C for 30h among all the materials. The weight gain was 5.10 mg.cm<sup>-2</sup>, a 36.2% improvement on the base alloy. On adding the SiC<sub>p</sub>, the corrosion weight of the material gradually decreased. This phenomenon indicates that the SiC<sub>p</sub> can

significantly reduce the corrosion weight of the material and improve thermal corrosion resistance. The 0.15vol.% GPLs reinforced composite became gradually stable after 20h of corrosion and entered the corrosion stabilization phase. The weight gains of 0.15vol.% GPLs sample was 7.10 mg.cm<sup>-2</sup> after the 30h corrosion. The addition of GPLs as reinforcements in the composite material also significantly improved the thermal corrosion resistance of the composite material.

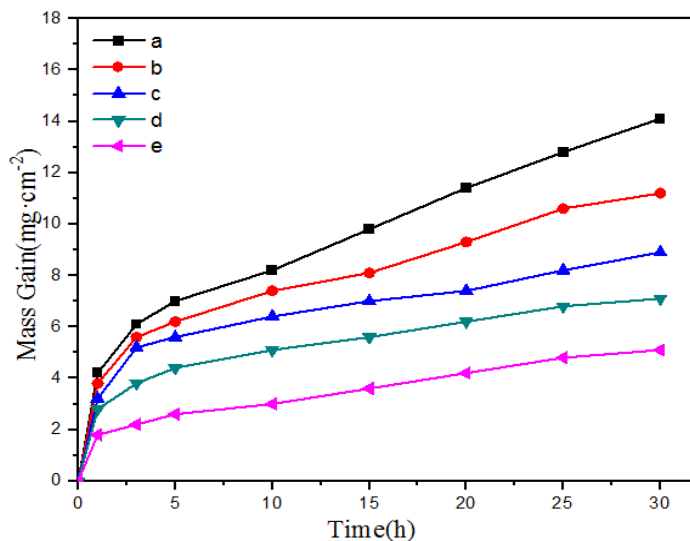
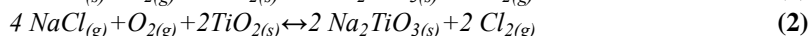
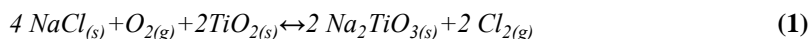


Fig. 3. The corrosion kinetics curve of matrix and composites corroded for 30h at 800 °C: (a) Sample A (b) Sample B (c) Sample C (d) Sample D (e) Sample E.

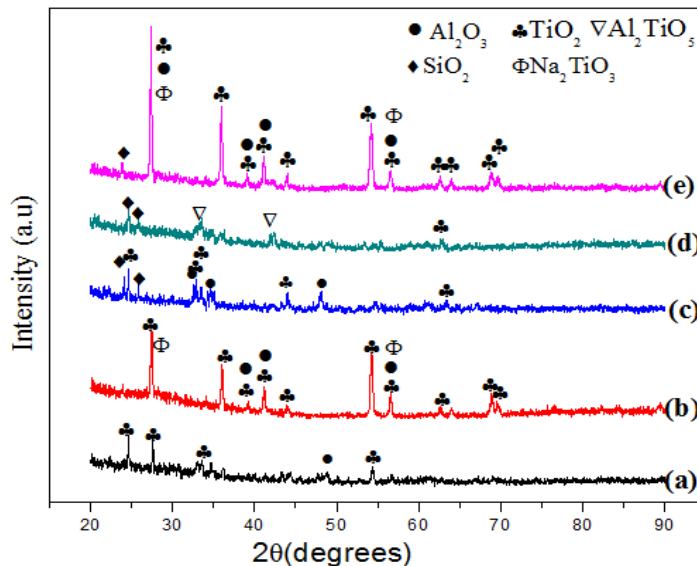
### Hot corrosion products and micro-morphology

Fig. 4 is the XRD pattern of the corrosion products of the matrix and the composites after corrosion at 800 °C for 30 hours. At the high-temperature environment of 800 °C, an oxidation reaction accompanied the corrosion reaction. Hence, the corrosion layer of the material contained oxidation and corrosion products. From the XRD pattern, the material's corrosion layer is mainly composed of rutile TiO<sub>2</sub>, Al<sub>2</sub>O<sub>3</sub>, and SiO<sub>2</sub> after thermal corrosion for 30 h in 25% NaCl + 75% Na<sub>2</sub>SO<sub>4</sub> mixed molten salt due to the presence of S and Na elements in the mixed molten salt. These elements reacted with the materials in the high-temperature corrosion environment to generate compounds such as Na<sub>2</sub>TiO<sub>3</sub> and Al<sub>2</sub>TiO<sub>5</sub>. From the map, the number and peak intensity of Na<sub>2</sub>TiO<sub>3</sub> is high because more TiO<sub>2</sub> got generated at high-temperature corrosive environments. The alkaline dissolution produced TiO<sub>2</sub><sup>-</sup>, which combined with free Na<sup>+</sup> to obtain Na<sub>2</sub>TiO<sub>3</sub> compounds according to Equations 1 and 2 [31]. Hence, the corrosion products of all the materials contained Na<sub>2</sub>TiO<sub>3</sub>.



Carefully observing the XRD pattern, the diffraction peak of SiO<sub>2</sub> in the corrosion products of SiCp reinforced composites was higher when compared with the base alloy. The peak strength of SiO<sub>2</sub> also increased further with the addition of the content SiCp, indicating more SiO<sub>2</sub> got generated in the material. Due to the dense structure of the generated SiO<sub>2</sub> oxide, the corrosion channel of the material got reduced, the penetration of corrosive elements was blocked, and the thermal corrosion resistance of the material improved significantly. The 5vol. % SiCp + 0.15vol. % GPLs sample had the weakest diffraction peak intensity of each corrosion product, indicating that

the addition of the reinforcements produced the least corrosion products on the surface, which is consistent with the smallest weight increase per unit area in the corrosion kinetic curve. Compared with the matrix, a small amount of  $\text{SiO}_2$  appeared in the composites with GPLs reinforcements. The  $\text{SiO}_2$  has good corrosion resistance, which can slow down the degree of thermal corrosion of the material to a certain extent.



**Fig. 4.** XRD patterns of matrix and composites corroded at 800°C for 30h: (a) Sample A (b) Sample B (c) Sample C (d) Sample D (e) Sample E.

Fig. 5 shows the SEM morphology of the substrate and the composite after thermal corrosion at 800 °C for 30 hours. From the figure, after four hours of high-temperature corrosion, the surface morphology of the materials was quite different. From Fig. 5 (a,b), the size and shape of the corrosion products of the base alloy are different, and there are relatively porous holes and cracks. Cracking and shedding of the corrosion products occurred in some areas, which caused the penetration of corrosion elements and reduced the material's resistance to thermal corrosion performance. From the high-magnification diagram, the corrosion products of the base alloy are mainly composed of a large number of short stick-shaped substances protruding outwards and some clusters of substances. The corrosion products are evenly distributed but with some cracks and holes. Compared with the matrix alloy, the corrosion layer of the 5vol.% SiCp reinforced composite was relatively flat and dense. The corrosion products are mainly needle-like, prismatic, and cluster-like substances. The morphology and size of the corrosion products are very different and mixed. The surface of the corrosion layer of the 5vol.% SiCp reinforced composite was relatively flat and dense, and the corrosion products contained outwardly growing prism-shaped substances of different sizes. The product prepared by adding more carbon through GPLs had the corroded surface of the composite materials mainly composed of a group of globular substances with small size and close arrangement.

As can be seen from the high magnification in Fig. 5 (j), the corrosion products are mainly short rod-like and cluster-like structures. The short rod-like structures are more evenly distributed on the cluster-like substances and are doped and fused. Table 3 shows the results of the EDS analysis of the corrosion products. From the table, the corrosion products are mainly Ti, Al, O, Na, and a small amount of S and Zr. According to the XRD analysis results, the corrosion products

of the material are mainly composed of  $\text{TiO}_2$ ,  $\text{Al}_2\text{O}_3$ ,  $\text{SiO}_2$ ,  $\text{Na}_2\text{TiO}_3$ , and  $\text{Al}_2\text{TiO}_5$ . However, due to the complicated corrosion process, the corrosion products may also contain  $\text{AlCl}_3$  and  $\text{TiS}$ .

**Table 3.** EDS element analysis of typical structure in Fig. 6.3.

	Sample A		Sample B		Sample C			Sample D			Sample E	
	1	2	1	2	1	2	3	1	2	3	1	2
B	-	-	0.05	0.04	-	-	-	-	-	-	-	-
C	-	5.31	0.98	0.42	2.25	0.77	0.60	4.28	2.33	1.66	4.79	6.47
O	37.99	35.96	29.68	25.66	36.60	22.32	39.83	44.80	38.06	33.08	42.64	45.61
Na	0.69	3.26	10.91	12.69	21.71	12.40	22.29	8.79	20.98	20.99	5.11	1.13
Al	6.17	5.12	0.03	0.13	0.67	-	16.16	-	0.58	0.24	10.27	9.33
Si	0.26	1.27	4.88	3.05	8.74	0.85	17.86	0.98	0.93	0.06	0.27	0.40
Zr	0.99	3.98	4.85	2.13	7.58	0.79	0.00	2.66	1.52	0.07	0.24	0.13
Nb	0.17	0.75	0.00	0.00	0.16	0.31	0.00	2.98	0.21	0.02	0.05	0.00
Mo	0.12	0.70	0.00	0.00	0.19	1.18	0.53	0.34	0.06	0.03	0.12	0.03
S	0.03	0.20	0.41	1.02	0.00	0.06	1.58	0.00	0.00	0.00	0.00	0.03
Cl	0.07	0.18	0.01	0.04	0.10	0.62	-	0.16	0.07	0.04	0.09	0.05
Sn	1.77	2.92	5.81	4.60	3.82	2.90	0.04	0.75	0.50	0.26	0.28	0.17
Ti	51.75	40.36	42.38	50.21	18.19	57.81	1.12	34.26	34.77	43.55	36.13	36.65

### Corrosion section and mechanism analysis

The cross-sectional morphology and line scanning of the base alloy and composites after corrosion at 800 °C for 30 hours is as shown in Fig. 6. From the figure, after 30 hours of high-temperature corrosion, the corrosion layers of all the materials did not fall off. The corrosion layers were relatively intact and combined well with the base material, showing good thermal corrosion resistance. Compared with composite materials, the thickness of the corrosion layer of the base alloy was thicker, about 72  $\mu\text{m}$ , with some holes distributed on the surface. Cracks also appeared in some areas, indicating that the thermal corrosion resistance of the base material was inferior to that of the composite materials. The corrosion kinetics of the materials was consistent. The thickness of the corrosion layer of the SiCp-reinforced composite was significantly smaller than that of the matrix alloy. The corrosion layer also became thinner, and the substrate tightly bonded. The thickness of the corrosion layer of the composite material with 5 vol. % SiCp, 5vol. % SiCp + 5vol. % SiCw, and 5vol. % SiCp + 0.15vol. % GPLs were about 37 $\mu\text{m}$ , 25 $\mu\text{m}$ , and 21 $\mu\text{m}$ , which are 51.4%, 34.7%, and 30.1 % of the base alloy. Similarly, the thickness of the corrosion layer of the composite material with 5vol. % SiCp + 1vol. %  $\text{B}_4\text{C}$  was about 37 $\mu\text{m}$ .

In the high-temperature environment, high-temperature oxidation accompanied the hot corrosion reaction. In the initial stage of the thermal corrosion reaction, the Al element in the material first reacted with O in the air under a high-temperature environment, forming a protective  $\text{Al}_2\text{O}_3$  oxide film. The  $\text{Al}_2\text{O}_3$  then covered the surface, which blocked O and other corrosive elements from the material to a certain extent. The internal diffusion improved the material's thermal corrosion performance. With the progress of the corrosion reaction, the protective effect of the  $\text{Al}_2\text{O}_3$  film weakened as the corrosion environment continued to be harsh.

Under high-temperature environments, the corrosion of molten salts produced a large amount of  $\text{Na}^+$  and  $\text{S}^{2-}$ . The  $\text{Na}^+$  combined with  $\text{TiO}^{2-}$  to produce  $\text{NaTiO}_2$ , and  $\text{S}^{2-}$  also reacted with  $\text{Ti}^{4+}$  to form  $\text{TiS}_2$ .  $\text{TiS}_2$  was reduced to  $\text{S}^{2-}$  under high-temperature and low-oxygen environments, and new  $\text{TiS}_2$  and  $\text{TiO}_2$  were generated inside the material. This process repeated, causing cyclic thermal corrosion of materials. Also, under the high-temperature environment, the element activity increased, the diffusion speed increased, and the rapid diffusion of the elements easily formed holes in the material. These were conducive to the entry and exit of corrosive elements and reduced corrosion resistance. The significant improvement in the corrosion resistance of the composite material compared to the base alloy may be due to the stable nature of the reinforcing phases, good corrosion resistance, and the role of grain refinement, which helped form a small and dense protective film. They also reduced the corrosion channel inside

the material, hindered the diffusion of corrosion elements, and improved the thermal corrosion resistance of the material.

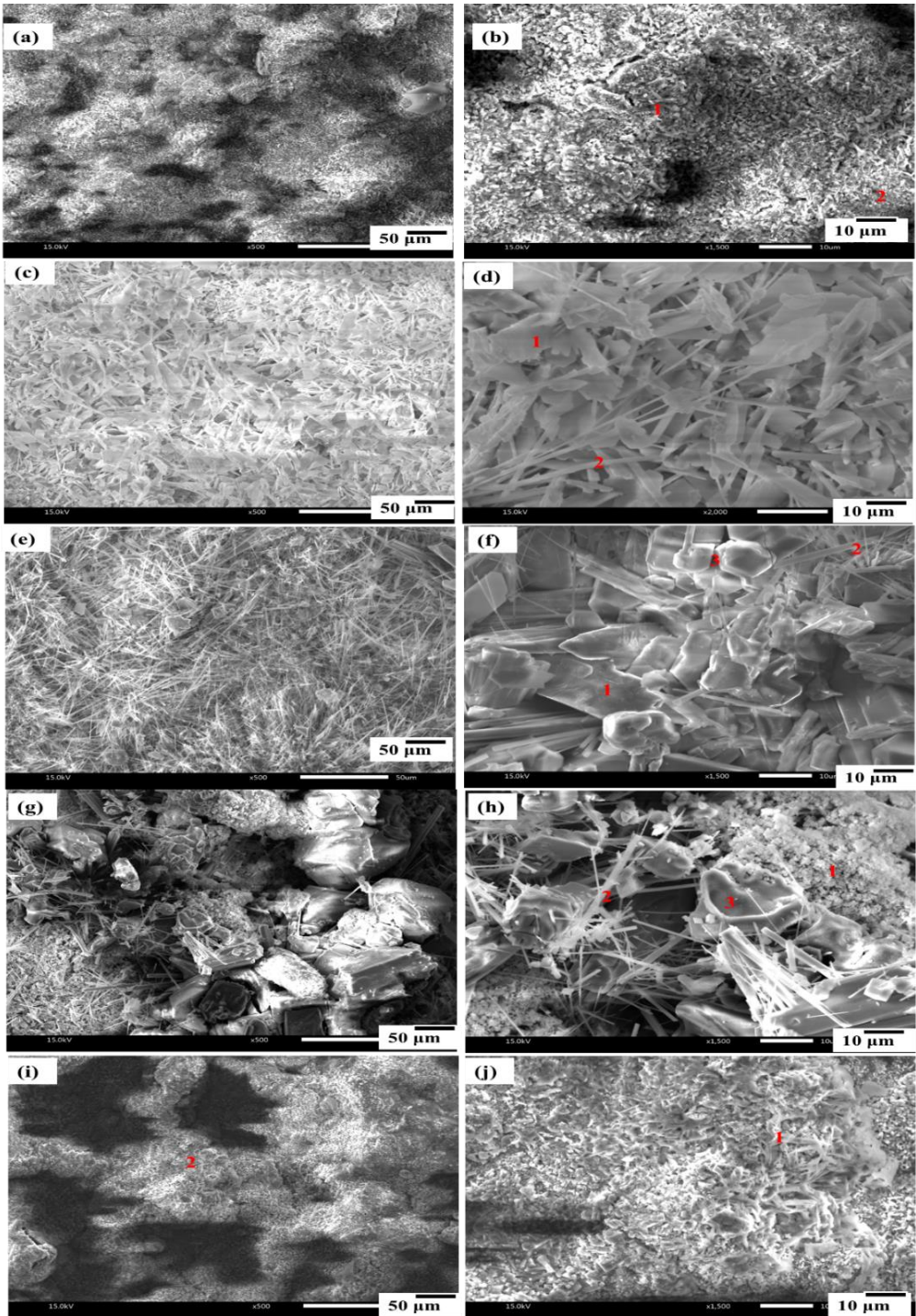


Fig. 5. The surface SEM morphology at low and high magnification of matrix and composites corroded

at 800°C for 30h: (a,b) Sample A (c,d) Sample B (e,f) Sample C (g,h) Sample D (i,j) Sample E.

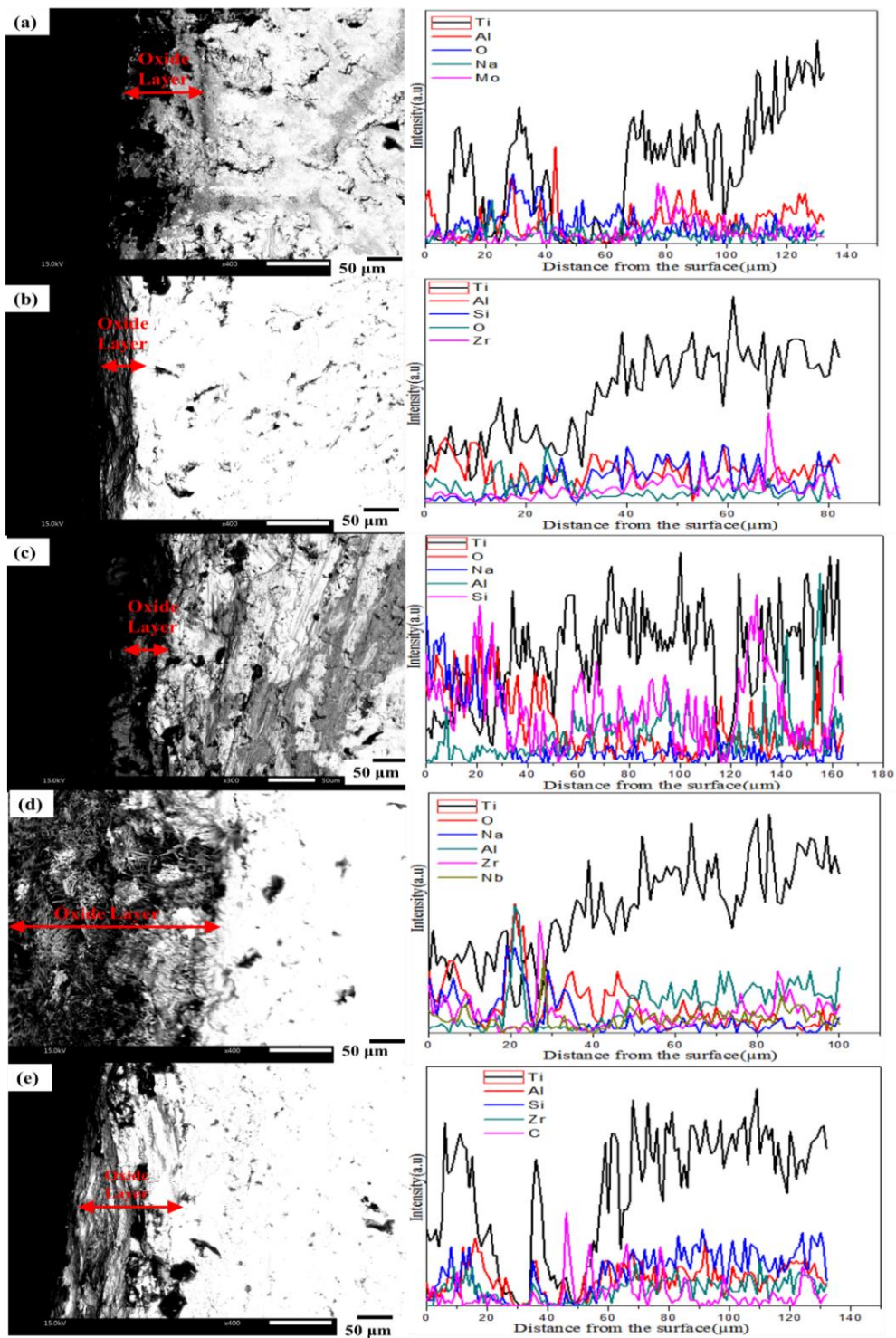


Fig. 6. Cross-section SEM morphology and elemental line scanning of material corroded

at 800°C for 30h: (a) Sample A (b) Sample B (c) Sample C (d) Sample D (e) Sample E.

## Conclusions

This paper used a 25% NaCl + 75% Na<sub>2</sub>SO<sub>4</sub> mixed molten salt as a corrosive medium to study the hot corrosion behavior of titanium alloy and its composite materials prepared by the SPS process discussed. The study found that:

- (i) The corrosion weight gain of the base material was significantly higher than that of the composite material, and the corrosion weight loss of the composite material decreased with the increase in the content of reinforcements. The corrosion gain of the base alloy after corrosion was 14.10 mg.cm<sup>-2</sup>. The corrosion gain of the 5vol.% SiCp reinforced composite has the lowest weight gain among the composites, with 5.1 mg.cm<sup>-2</sup>, which is 36.17% of the base alloy. As the corrosion temperature increased, the corrosion weight of the material increased, and the corrosion weight curve of the material at 800 °C was completely parabolic. The corrosion weight gain was relatively slow.
- (ii) The corrosion products of all the materials were similar and mainly composed of TiO<sub>2</sub>, Al<sub>2</sub>O<sub>3</sub>, Na<sub>2</sub>TiO<sub>3</sub>, and Al<sub>2</sub>TiO<sub>5</sub>. Also, the content of SiCp strengthened the peak of SiO<sub>2</sub> in the composite material, indicating that more protective SiO<sub>2</sub> was generated, which can improve the thermal corrosion resistance of the material to a certain extent.
- (iii) After corrosion at 800 °C for 30 hours, no distinct peeling-off of the corrosion layers of the 5vol.% SiCp reinforced composite material was observed. The corrosion layers were flat and dense, well bonded to the substrate, and the material had better thermal corrosion resistance. The corrosion products of the base material at 800 °C have a partial shedding, and deep cracks and holes appeared in local areas, which caused the infiltration and diffusion of corrosive elements, weakening the material's thermal corrosion resistance.

## Acknowledgements

This work was supported by the Key Projects of the 13th Five-Year Plan Equipment Pre-research Foundation of the Ministry of Equipment Development of the Central Military Commission of China (No: 6140922010201).

## References

- [1] Y. Yu, Y.H. Cai, X.H. Chen, T. Wang, Y.D. Wu, J.J. Si, X.D. Hui, A high strength and elastic carbon containing near- $\alpha$  Ti alloy prepared by hot isostatic pressing process, *Materials Science and Engineering: A*, **651(1)**, 2016, pp. 961-967
- [2] X. Sun, H. Li, Y. Han, J. Li, J. Mao, W. Lu, Compressive response and microstructural evolution of bimodal sized particulates reinforced (TiB+ La<sub>2</sub>O<sub>3</sub>)/Ti composites, *Journal of Alloys and Compounds*, **732**, 2018, pp. 524-535
- [3] J. Dai, J. Zhu, C. Chen, F. Weng, High temperature oxidation behavior and research status of modifications on improving high temperature oxidation resistance of titanium alloys and titanium aluminides: A review, *Journal of Alloys and Compounds*, **685**, 2016, pp. 784-798
- [4] V.M. Tabie, C. Li, W. Saifu, J. Li, X. Xu, Mechanical properties of near alpha titanium alloys for high-temperature applications-a review, *Aircraft Engineering and Aerospace Technology*, **92(4)**, 2020, pp. 521-540
- [5] M. Thomas, B. Wynne, W. Rainforth, An alternative method to separate and analyse the microtextures and microstructures of primary alpha grains and transformed beta grains in near- $\alpha$  titanium alloy Timetal 834, *Materials characterization*, **55(4-5)**, 2005, pp. 388-394

- [6] T. Moskalewicz, B. Dubiel, B. Wendler, AlCuFe (Cr) and AlCoFeCr coatings for improvement of elevated temperature oxidation resistance of a near- $\alpha$  titanium alloy, *Materials characterization*, **83**, 2013, pp. 161-169
- [7] W.-J. Zhang, X.-Y. Song, S.-X. Hui, W.-J. Ye, W.-Q. Wang, Phase precipitation behavior and tensile property of a Ti–Al–Sn–Zr–Mo–Nb–W–Si titanium alloy, *Rare metals*, **37(12)**, 2018, pp. 1064-1069
- [8] Y. Diao, X. Song, W. Zhang, M. Zhao, W. Ye, S. Hui, Microstructure and Mechanical Properties of a Ti–Al–Sn–Zr–Mo–Nb–W–Si High-Temperature Titanium Alloy, Chinese Materials Conference, 2018, Springer, pp 85-91
- [9] Y.-L. Wang, X.-Y. Song, W. Ma, W.-J. Zhang, W.-J. Ye, S.-X. Hui, Microstructure and tensile properties of Ti-62421S alloy plate with different annealing treatments, *Rare Metals*, **37(7)**, 2018, pp. 568-573
- [10] Y. Liu, Z. Chen, T. Jin, L. Chai, Present situation and prospect of 600°C high temperature titanium alloys, *Materials Reports*, **32(11)**, 2018, pp. 1863-1869
- [11] S. Kirklin, J.E. Saal, V.I. Hegde, C. Wolverton, High-throughput computational search for strengthening precipitates in alloys, *Acta Materialia*, **102**, 2016, pp. 125-135
- [12] J. Zhang, D. Li, Effect of Al content on precipitation of  $\alpha_2$  ordered phase in Ti-Al-Sn-Zr-Mo-Si-Nd alloys, *Journal of Materials Science and Technology -Shenyang-*, **18**, 2002, pp. 245-247
- [13] J. Murugesan, D. Ping, Y. Yamabe-Mitarai, Effect of Zr Addition on High Temperature Mechanical Properties of Near Alpha Ti-Al-Zr-Sn Based Alloy, *Materials Science Forum*, **783-786**, 2014, pp. 580-583
- [14] B. Fu, H. Wang, C. Zou, Z. Wei, The effects of Nb content on microstructure and fracture behavior of near  $\alpha$  titanium alloys, *Materials & Design (1980-2015)*, **66**, 2015, pp. 267-273
- [15] C. Chen, Z. Chen, S. Zhu, J. Liu, Q. Wang, Solution Temperature Sensitivity for Primary  $\alpha$ -Phase Volume Fraction of Ti750 Alloys, *Chinese Journal of Materials Research*, **33(10)**, 2019, pp. 794-800
- [16] T. Kitashima, K. Suresh, Y. Yamabe-Mitarai, Effect of germanium and silicon additions on the mechanical properties of a near- $\alpha$  titanium alloy, *Materials Science and Engineering: A*, **597**, 2014, pp. 212-218
- [17] C. Poletti, G. Hölbl, Mechanical properties of particle reinforced titanium and titanium alloys, *Kovove Mater*, **48**, 2010, pp. 87-95
- [18] Y. Qin, W. Lu, D. Zhang, J. Qin, B. Ji, Oxidation of in situ synthesized TiC particle-reinforced titanium matrix composites, *Materials Science and Engineering: A*, **404(1-2)**, 2005, pp. 42-48
- [19] Y.-J. Kim, P. Yadav, J. Hahn, X. Xiao, D.B. Lee, Oxidation of titanium matrix composites reinforced with (TiB+ TiC) particulates, *Metals and Materials International*, **25(3)**, 2019, pp. 627-632
- [20] V.M. Tabie, X. Xu, M.K. Osman, J. Li, Oxidation performance of particle-reinforced Ti750 matrix composites, *Proceedings of the Institution of Mechanical Engineers, Part L: Journal of Materials: Design and Applications*, 2022, pp. 14644207221126996
- [21] K.S. Prakash, P. Gopal, D. Anburose, V. Kavimani, Mechanical, corrosion and wear characteristics of powder metallurgy processed Ti-6Al-4V/B4C metal matrix composites, *Ain Shams Engineering Journal*, **9(4)**, 2018, pp. 1489-1496
- [22] X. Yang, Z.-y. Zhang, B. Wang, W.-j. Ma, W.-l. Wang, W.-g. Chen, N.-n. Kang, S.-f. Liu, Microstructure, mechanical properties and corrosion performance of selective laser melting Ti/GNPs composite with a porous structure, *Journal of Central South University*, **28(8)**, 2021, pp. 2257-2268
- [23] T. Zhao, S. Zhang, F.Q. Zhou, H.F. Zhang, C.H. Zhang, J. Chen, Microstructure evolution and properties of in-situ TiC reinforced titanium matrix composites coating

- by plasma transferred arc welding (PTAW), *Surface and Coatings Technology*, **424**, 2021, pp. 127637
- [24] Z.Z. Fang, J.D. Paramore, P. Sun, K.R. Chandran, Y. Zhang, Y. Xia, F. Cao, M. Koopman, M. Free, Powder metallurgy of titanium—past, present, and future, *International Materials Reviews*, **63(7)**, 2018, pp. 407-459
- [25] W. Lee, J. Seong, Y. Yoon, C. Jeong, C. Van Tyne, H. Lee, S. Chang, Synthesis of TiC reinforced Ti matrix composites by spark plasma sintering and electric discharge sintering: A comparative assessment of microstructural and mechanical properties, *Ceramics International*, **45(7)**, 2019, pp. 8108-8114
- [26] O.E. Falodun, B.A. Obadele, S.R. Oke, A.M. Okoro, P.A. Olubambi, Titanium-based matrix composites reinforced with particulate, microstructure, and mechanical properties using spark plasma sintering technique: a review, *The International Journal of Advanced Manufacturing Technology*, **102(5)**, 2019, pp. 1689-1701
- [27] M. Lagos, I. Agote, G. Atxaga, O. Adarraga, L. Pambaguian, Fabrication and characterisation of titanium matrix composites obtained using a combination of self propagating high temperature synthesis and spark plasma sintering, *Materials Science and Engineering: A*, **655**, 2016, pp. 44-49
- [28] G.Y. Lai, High temperature corrosion of engineering alloys, 1990
- [29] V.M. Tabie, J.K. Quaisie, J. Li, P. Yamba, X. Xu, Microstructure and mechanical properties of particle reinforced high-temperature titanium composites, *Eur. Phys. J. Appl. Phys.*, **98**, 2023, pp. 3
- [30] X. Xu, C. Li, V.M. Tabie, S. Wang, C. Cai, Y. Liu, Y. Xiao, S. Huang, Microstructure and properties of Ti-Al-Sn-Zr-Nb-Si matrix composite reinforced with in-situ TiC and Ti<sub>5</sub>Si<sub>3</sub> prepared by powder metallurgy, *Materials Research Express*, **6(10)**, 2019, pp. 1065b1063
- [31] C. Ciszak, I. Popa, J.-M. Brossard, D. Monceau, S. Chevalier, NaCl induced corrosion of Ti-6Al-4V alloy at high temperature, *Corrosion Science*, **110(9)**, 2016, pp. 91-104

---

Received: November 10, 2022

Accepted: January 22, 2023